

A PLETHORA OF AGN AMONG Ly α GALAXIES AT LOW REDSHIFT¹

STEVEN L. FINKELSTEIN^{2,*}, SETH H. COHEN³, SANGEETA MALHOTRA³, JAMES E. RHOADS³ & CASEY PAPOVICH²
Draft version April 20, 2019

ABSTRACT

We investigate the fraction of $z \sim 0.3$ Lyman alpha emitting galaxies (LAEs) which host active galactic nucleus activity, which is typically from 1 – 5% at $2 \lesssim z \lesssim 4.5$. Using optical spectroscopy of 23 LAEs at $0.2 \leq z \leq 0.45$ selected with GALEX UV data, we probed for AGN with a variety of methods, including line widths, diagnostic line ratios, high-ionization emission, X-ray luminosity and infrared activity. We found that our sample of low-redshift LAEs has an AGN fraction of $43^{+18}_{-26}\%$, significantly higher than at high redshift. While previous results have shown that low-redshift LAEs have a lower space density than their high-redshift analogs, these results show that star-forming LAEs at low-redshift are rarer still. Accounting for differences in available AGN classification methods, we conclude that rest-frame optical spectroscopy is necessary to exclude AGN contamination in LAEs at high redshift, and that current estimates of the AGN fraction in high-redshift LAEs are at best lower limits.

Subject headings: galaxies: active – galaxies: evolution

1. INTRODUCTION

Lyman alpha (Ly α) emitting galaxies (LAEs) have been used for years as probes of the high-redshift universe (e.g., Cowie & Hu 1998; Rhoads et al. 2000; Malhotra & Rhoads 2002; Ouchi et al. 2005, 2008; Gawiser et al. 2006b; Gronwall et al. 2007; Pirzkal et al. 2007; Nilsson et al. 2007, 2009; Finkelstein et al. 2007, 2008, 2009a). These studies have shown that LAEs are fairly common from $2 \leq z \leq 7$, and more interestingly, their properties do not evolve strongly with time, with stellar populations and Ly α luminosity functions which are roughly constant over this redshift range.

Deharveng et al. (2008) discovered a sample of ~ 100 low-redshift LAEs from $0.2 \leq z \leq 0.45$ with the Galaxy Evolution Explorer (GALEX). They ruled out objects with Ly α line widths $> 1200 \text{ km s}^{-1}$ as broad-lined active galactic nuclei (AGN), although they typically could not rule out narrow-lined AGN, as the C III or C IV diagnostic lines were either too faint, or located in a noisy part of the spectrum. They found that the Ly α luminosity function of these objects was substantially different than at high-redshift, with low-redshift LAEs having a lower surface density and being typically less luminous in the Ly α line. In Finkelstein et al. (2009b), we studied the physical properties of 30 of these LAEs, and found them to be significantly different than their high-redshift counterparts, with typical ages of a few Gyr, and stellar masses of $\sim 10^{10} M_{\odot}$. We found that a few could harbor AGN, but with only one object detected in X-rays, we could not discern AGNs from star-forming galaxies. In this Letter, we present an optical spectroscopic study of 23 of these low-redshift LAEs in order to determine the AGN fraction in LAEs at this redshift. While Deharveng et al. have already ruled out most broad-

lined AGN, optical spectroscopy will enable us to search for narrow-lined AGN. Where applicable, we assume $H_0 = 70 \text{ km s}^{-1} \text{ Mpc}^{-1}$, $\Omega_m = 0.3$ and $\Omega_{\Lambda} = 0.7$ (c.f. Spergel et al. 2007).

2. DATA

2.1. Observations and Data Reduction

We obtained spectroscopy of 23 low-redshift LAEs in the Extended Groth Strip (EGS), using the Hectospec at the 6.5m MMT, which has 300 1.5'' fibers covering a 1° diameter field-of-view (Fabricant et al. 2005). We obtained 2 hours of spectroscopy on 19 March 2009, with spectral coverage from $\sim 3650 - 9200 \text{ \AA}$, and a spectral resolution of $\sim 5 \text{ \AA}$. We used the External SPECROAD⁵ pipeline for data reduction (developed by Juan Cabanela; private communication). This pipeline performs standard spectroscopic reductions, including bias, dark and flat correction, and wavelength calibration (rms residuals $\approx 0.1 \text{ \AA}$). We flux-calibrated the spectra using observations of Sloan Digital Sky Survey (SDSS) F-type stars. Further details on the observations and data reduction will be presented in a future paper (Finkelstein et al. 2009, in prep).

2.2. Line Fitting

The 23 objects varied in redshift from $0.2 \lesssim z \lesssim 0.45$, thus we found 31 possible spectral lines which we could detect, from Mg II $\lambda\lambda$ 2796, 2803 to [S II] λ 6733. We examined the expected position (using the redshift from Deharveng et al. (2008) as a first estimate) of each of the expected lines in each spectrum, and noted whether it was detected, and whether it was observed in emission or absorption. We fit a Gaussian curve to each detected line, using the MPFIT IDL software package⁶, obtaining the continuum flux, central wavelength, Gaussian σ and line flux. Errors on each of these parameters were estimated via Monte Carlo simulations by varying each spectral data point within its photometric uncertainty.

3. RESULTS

Figure 1 shows spectra of two of the observed LAEs, one which we classify as an AGN, and one which appears

¹ Observations reported here were obtained at the MMT Observatory, a joint facility of the University of Arizona and the Smithsonian Institution. These observations were also based in part on observations made with the NASA Galaxy Evolution Explorer. GALEX is operated for NASA by the California Institute of Technology under NASA contract NAS5-98034.

² George P. and Cynthia W. Mitchell Institute for Fundamental Physics and Astronomy, Department of Physics, Texas A&M University, College Station, TX 77843

³ School of Earth and Space Exploration, Arizona State University, Tempe, AZ 85287

* stevenf@physics.tamu.edu

⁵ <http://iparrizar.mnstate.edu/~juan/research/ESPECROAD/index.php>

⁶ <http://cow.physics.wisc.edu/~craigm/idl/idl.html>

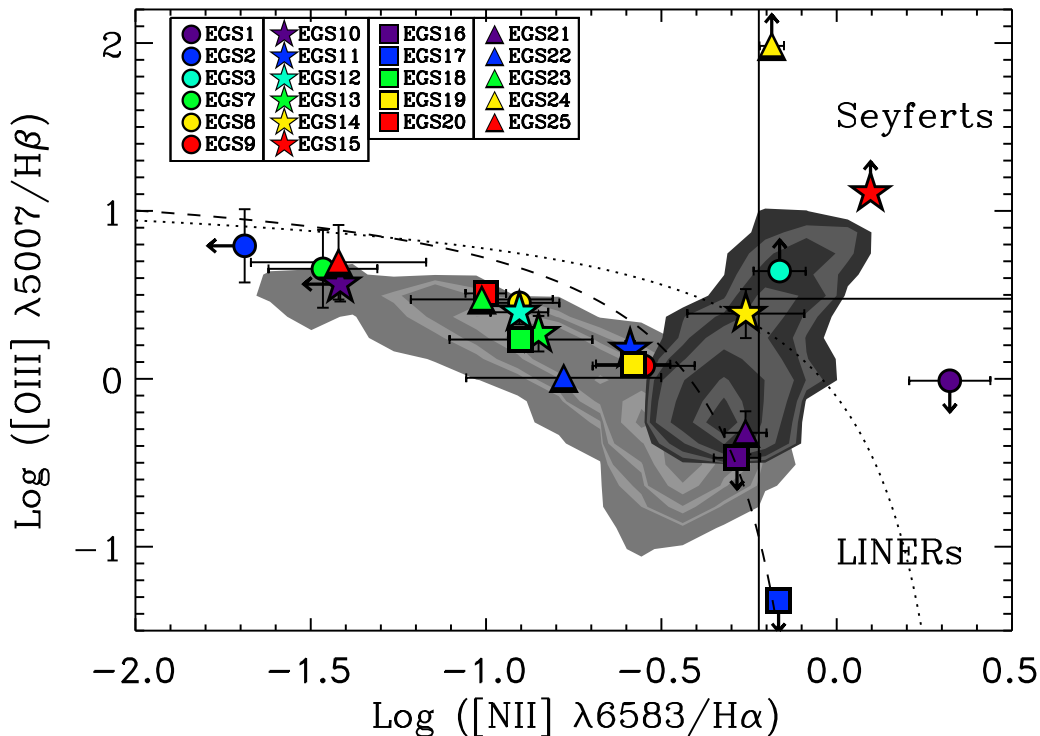


FIG. 2.— Our 23 LAEs plotted on the standard BPT line ratio diagram. When a given line is undetected, we plot a 3σ upper limit. The light and dark gray contours represent the star-forming and AGN sequences, respectively, from SDSS data, with the star-forming contours representing 2, 15, 25, 60, 100, 300 and 500 galaxies per 0.03×0.03 dex bin, and the AGN contours representing 5, 8, 12, 20, 40, 75 and 100 AGNs per bin. The dotted line is the maximum starburst curve from Kewley et al. (2001), while the dashed curve is an updated SF/AGN demarcation line from Kauffmann et al. (2003). The solid lines denote regions expected to be inhabited by Seyferts and LINERs (Kauffmann et al. 2003).

star-forming sequence, and significantly higher than the maximum starburst curve.

EGS16, EGS17 and EGS21 lie in regions which could correspond to either AGN or star-forming galaxies, as well as near the Kauffmann et al. demarcation line. EGS16 and EGS17 have detected [Ne V] emission. As EGS21 was not indicated by any of our previous methods, thus we also only consider it a possible AGN.

Baldwin, Phillips, & Terlevich (1981) also derived classifications using lines of O I and [O II], and their Fig. 4, which plots O I $\lambda 6300/H\alpha$ versus [O II]/[O III], shows a clear separation in O I $\lambda 6300/H\alpha$, with nearly all power-law ionization objects (i.e. AGN) having $\log(O I/H\alpha) \gtrsim -1$, and all star-forming objects having $\log(O I/H\alpha) \lesssim -1.5$. We find that out of the five objects which have $\geq 3\sigma$ detections of O I $\lambda 6300$, EGS10 and EGS24 exhibit $\log(O I/H\alpha)$ indicative of AGN activity, of -0.74 and -1.05, respectively (the remaining three objects all had $\log(O I/H\alpha) \lesssim -1.4$). EGS10 was not indicated by any of our previous classification methods, thus we now regard it as a possible AGN.

3.4. X-rays

We examined the positions of each of our LAEs in the AEGIS-X 200 ksec *Chandra* point source catalog (v2.0; Laird et al. (2009)). We found that only EGS9 has a X-ray counterpart within $5''$ (a separation of $r < 0.19''$). The closest counterpart to the remaining objects is at a separation of $18''$, thus they are X-ray undetected. The full-band X-ray flux of EGS9 is $4.39 \pm 0.79 \times 10^{-15}$ erg s^{-1} cm^{-2} , which at the newly derived redshift of $z = 0.246$ corresponds to $L_{FB} = 8.0 \pm 1.5 \times$

10^{41} erg s^{-1} . This detection alone is not definitive proof of an AGN, as star-forming galaxies typically show $L_{FB} < 10^{42}$ erg s^{-1} , thus these X-rays could be due to star-formation, a low-luminosity AGN, or some combination. However, the emission detected at $24 \mu m$ (see §3.5) could imply that dust is obscuring some of the X-rays. The obscuration is corroborated by the hardness ratio of -0.13, which when combined with the X-ray luminosity, satisfies the Szokoly et al. (2004) AGN criteria, thus we regard EGS9 as a probable AGN. We note that an object similar to EGS9 at high-redshift likely would not be selected as an AGN via its X-ray flux, as its X-ray/Ly α flux ratio of ~ 1.2 is much less than the typical limit from the Large Area Lyman Alpha (LALA; Rhoads et al. (2000)) survey of < 10 .

3.5. Infrared

The AEGIS-X catalog has limiting luminosities of $L_{0.5-2keV} = 1.5 \times 10^{40}$ and $L_{2-10keV} = 1.1 \times 10^{41}$ erg s^{-1} , assuming $z = 0.3$, thus if the objects in our sample had typical AGN X-ray luminosities, we should be able to detect them. However, this can be understood given the unification picture of AGN (e.g., Urry & Padovani 1995), where one typically has a direct line-of-sight to see the X-rays from the accretion disk. When observing from other angles, the accretion disk can be blocked by the torus of dust and gas surrounding the center. In this case, the dust emission from the torus may be visible at long wavelengths.

Stern et al. (2005) defined a color-color region using colors from the *Spitzer* Infrared Array Camera (IRAC) which preferentially selects AGN in the redshift range of our sample (20%

TABLE 1
MEASURED OBJECT PROPERTIES

Object	ID	Redshift	FWHM _P (km s ⁻¹)	24 μm Flux (mJy)	AGN Grade	Class Method
EGS1	32462	0.1996	—	—	B	3
EGS2	7430	0.2078	221 ± 1	0.23 ± 0.02	B	2
EGS3	5087	0.2102	155 ± 48	—	B	3
EGS7	18322	0.2440	220 ± 1	0.16 ± 0.01	SF	—
EGS8	2682	0.2395	206 ± 5	—	SF	—
EGS9	5715	0.2462	276 ± 6	0.20 ± 0.01	B	4
EGS10	17005	0.2466	223 ± 3	—	C	3
EGS11	4719	0.2524	189 ± 4	0.14 ± 0.01	SF	—
EGS12	21404	0.2515	194 ± 3	—	SF	—
EGS13	12279	0.2607	234 ± 2	0.30 ± 0.03	SF	—
EGS14	14069	0.2578	229 ± 13	—	A	2,3
EGS15	21024	0.2630	174 ± 29	0.23 ± 0.02	B	3
EGS16	3488	0.2643	211 ± 12	—	A	2,3
EGS17	3525	0.2647	244 ± 13	0.62 ± 0.06	A	2,3
EGS18	29573	0.2689	200 ± 10	—	B	2
EGS19	31403	0.2666	200 ± 3	—	SF	—
EGS20	33559	0.2680	210 ± 3	—	C	2
EGS21	9045	0.2814	229 ± 7	—	C	3
EGS22	21579	0.2828	245 ± 9	0.16 ± 0.01	SF	—
EGS23	28751	0.2865	264 ± 2	—	SF	—
EGS24	23096	0.3025	1064 ± 17	—	A	1,2,3
EGS25	29558	0.3243	240 ± 1	—	SF	—
EGS27	10182	0.4512	257 ± 2	0.29 ± 0.01	C	5

NOTE. — The second column is the ID number from Deharveng et al. (2008). The redshift is the weighted mean of all lines detected at $\geq 3\sigma$ significance for each object. The characteristic error on the redshifts is $\Delta z \sim .00001$. FWHM_P represents the full width at half maximum of detected lines of hydrogen and helium. The AGN classification grades refer to our level of confidence in the classification. A grade of A was given when two or more methods implied AGN activity, while B means that only one classification implied AGN activity, and C means that the object had only marginal evidence for AGN activity. SF denotes that the object appears to be dominated by star formation. The last column denotes the method which classified a particular object: 1=Line width, 2=Highly ionized line emission, 3=BPT line ratios, 4=X-rays and 5=IRAC color.

contamination), due to the rising power law spectrum (i.e. from warm dust) exhibited by these objects. We examined the AEGIS IRAC catalog and found that four of our objects were covered by the IRAC data: EGS1, EGS9, EGS15 and EGS27. Of these, only EGS27 lies within the selection wedge, and only $\sim 1\sigma$ from the edge. Thus, we regard EGS27 as a possible AGN. Even though other methods select the remaining three objects as AGN, they all reside outside the wedge.

We also examined the Multiband Imaging Photometer for Spitzer (MIPS) 24 μm catalog from the Far-Infrared Deep Extragalactic Legacy (FIDEL) survey (Dickinson et al. 2009, in prep), which would detect emission from slightly cooler dust, which could indicate that a dusty torus is attenuating the X-ray flux. However a non-detection does not dispute the classification of an AGN, it could just indicate that the MIR flux is weak. On the flip-side, a 24 μm detection from a non-AGN does not necessarily indicate AGN activity, as the dust can also be heated due to star-formation activity, which is observable at these redshifts. Of the 13 LAEs covered by MIPS, nine had $> 3\sigma$ detections at 24 μm, listed in Table 1. Five of these are classified as definite/possible AGNs: EGS2, EGS9, EGS15, EGS17 and EGS27. It thus appears likely that these objects have a dusty torus which is attenuating the X-ray flux, with EGS9 still showing weak X-ray flux possibly due to an intrinsically large X-ray photon budget.

4. DISCUSSION

4.1. Final Classification

We now assign a confidence level to each of the objects which we have classified as an AGN. Objects which have been indicated by two or more methods are given a classification grade of “A”; objects with unambiguous classification via one method, but not in any other are given a grade of “B”; and objects which have only a possible classification within one method are given a grade of “C.” As shown in Table 1, we have 4 grade A, 6 grade B and 4 grade C AGNs. Taking our A & B classifications as being reliably indicative of AGN activity, we find an AGN fraction of 43% (10/23) in low-redshift LAEs. Including class C AGNs, this could be as high as 61% (14/23), while neglecting class B & C AGNs provides a minimum value of 17% (4/23).

4.2. Evolution in LAE AGN Fraction?

Expanding upon initial work by Malhotra et al. (2003), Wang et al. (2004) examined the positions of ~ 100 known $z \sim 4.5$ LAEs from the LALA survey in *Chandra* X-ray data, and detected none of their LAEs, even when stacked, with a stacked 3σ upper limit of $L \leq 2.8 \times 10^{42}$ erg s⁻¹, concluding that less than 4.8% of their high-redshift LAEs could be AGNs. Dawson et al. (2004) and Wang et al. (2009, in prep) examined many of these same LAEs with optical (rest-frame ultraviolet) spectroscopy, and also found no evidence for AGN activity, with Wang et al. reporting an upper limit on the AGN fraction of $< 17\%$ from the upper limit on the CIV $\lambda 1549$ emission line. Studying a sample of 40 LAEs at $z \sim 3.1$ from the Multiwavelength Survey by Yale Chile (MUSYC; Gawiser et al. (2006a)), Gawiser et al. (2006b) detected one LAE in the deep *Chandra* data publicly available in the Extended *Chandra* Deep Field – South (CDF–S), yielding an estimated AGN fraction of $2\% \pm 2\%$ among $z \sim 3.1$ LAEs. Converting the upper limit of an X-ray stack of the remaining objects to a star formation rate, they found it to be consistent with their stellar population modeling-based SFR, implying no further AGN contamination. Nilsson et al. (2009) found that 15 among their sample of 170 $z = 2.25$ LAEs had X-ray counterparts, concluding that the AGN fraction in LAEs at $z \sim 2.25$ is at least 5%. Lehmer et al. (2009) also found an increase in the LAE AGN fraction, finding 5.1% of their 158 $z = 3.09$ LAEs hosted AGN. However, these objects are located in the SSA22 field, which is known to have a forming proto-cluster at this redshift, and Lehmer et al. attribute the rise in AGN fraction to enhanced merger activity and supermassive black hole growth due to the overdense cluster environment.

The AGN fraction of $43^{+18\%}_{-26\%}$ for $z \sim 0.3$ LAEs is greatly enhanced from even the cluster environment at $z = 3.09$ (Lehmer et al. 2009). We thus conclude that the fraction of LAEs at low-redshift which host AGN may have evolved strongly from that at $z > 2$, which has strong implications on the nature of LAEs, which do not change much from $2 < z < 7$. Their strong evolution in both stellar population (Finkelstein et al. 2009b) and AGN fraction shows that low-redshift LAEs represent a far more evolved class of object, while the unchanging high- z LAEs likely represent the true building blocks of present-day galaxies.

However, we also note that at most three of our methods (line widths, X-rays and high-ionization emission) have been used in LAEs at high redshift. Reclassifying with only these methods, we obtain an AGN fraction of 26%, perhaps better suited to comparisons with high-redshift, although even the high-redshift studies which probe the rest-frame UV may still

miss AGN, as lines such as C IV $\lambda 1549$ could be heavily attenuated if dust is present, while rest-frame optical lines will be less attenuated. We can see that when restricted to measurements available at high-redshift we can miss anywhere from $\sim 15 - 40\%$ of the AGNs in our sample. We thus conclude that high-redshift LAE AGN fraction measurements may be at best lower limits, and this highlights the need for infrared spectroscopy and deep, high-resolution IR imaging to detect

the true AGN fraction in LAEs at high redshift, available in the not too distant future with the *James Webb Space Telescope*.

This work was supported by GALEX Archival Grant #GI5-036 and the Texas A&M University College of Science and Department of Physics.

REFERENCES

- Baldwin, J. A., Phillips, M. M., & Terlevich, R. 1981, *PASP*, 93, 5
 Cowie, L. L., & Hu, E. M. 1998, *AJ*, 115, 1319
 Davis, M., et al. 2007, *ApJ*, 660, L1
 Dawson, S., et al. 2004, *ApJ*, 617, 707
 Deharveng, J.-M., et al. 2008, *ApJ*, 680, 1072
 Fabricant, D., et al. 2005, *PASP*, 117, 1411
 Finkelstein, S. L., Cohen, S. H., Malhotra, S., & Rhoads, J. E. 2009b, *ApJ* in press
 Finkelstein, S. L., Rhoads, J. E., Malhotra, S., & Grogin, N. 2009a, *ApJ*, 691, 465
 Finkelstein, S. L., Rhoads, J. E., Malhotra, S., Grogin, N., & Wang, J. 2008, *ApJ*, 678, 655
 Finkelstein, S. L., Rhoads, J. E., Malhotra, S., Pirzkal, N., & Wang, J. 2007, *ApJ*, 660, 1023
 Gawiser, E., et al. 2006a, *ApJS*, 162, 1
 —. 2006b, *ApJ*, 642, L13
 Gronwall, C., et al. 2007, *ApJ*, 667, 79
 Kauffmann, G., et al. 2003, *MNRAS*, 346, 1055
 Kewley, L. J., Dopita, M. A., Sutherland, R. S., Heisler, C. A., & Trevena, J. 2001, *ApJ*, 556, 121
 Laird, E. S., et al. 2009, *ApJS*, 180, 102
 Lehmer, B. D., et al. 2009, *ApJ*, 691, 687
 Malhotra, S., & Rhoads, J. E. 2002, *ApJ*, 565, L71
 Malhotra, S., Wang, J. X., Rhoads, J. E., Heckman, T. M., & Norman, C. A. 2003, *ApJ*, 585, L25
 Nilsson, K. K., Tapken, C., Möller, P., Freudling, W., Fynbo, J. P. U., Meisenheimer, K., Laursen, P., & Östlin, G. 2009, *A&A*, 498, 13
 Nilsson, K. K., et al. 2007, *A&A*, 471, 71
 Osterbock, D. E. 1989, *Astrophysics of Gaseous Nebulae and Active Galactic Nuclei* (Mill Valley: University Science Books)
 Ouchi, M., et al. 2005, *ApJ*, 620, L1
 —. 2008, *ApJS*, 176, 301
 Pirzkal, N., Malhotra, S., Rhoads, J. E., & Xu, C. 2007, *ApJ*, 667, 49
 Rhoads, J. E., Malhotra, S., Dey, A., Stern, D., Spinrad, H., & Jannuzi, B. T. 2000, *ApJ*, 545, L85
 Shapley, A. E., Steidel, C. C., Pettini, M., & Adelberger, K. L. 2003, *ApJ*, 588, 65
 Spergel, D. N., et al. 2007, *ApJS*, 170, 377
 Stern, D., et al. 2005, *ApJ*, 631, 163
 Szokoly, G. P., et al. 2004, *ApJS*, 155, 271
 Urry, C. M., & Padovani, P. 1995, *PASP*, 107, 803
 Wang, J. X., et al. 2004, *ApJ*, 608, L21